5

Regularity Analysis of Airborne Natural Gamma Ray Data Measured in the Hoggar Area (Algeria)

Saïd Gaci[1], Naïma Zaourar[1], Louis Briqueu[2] and Mohamed Hamoudi[1]

[1]*University of Sciences and Technology Houari Boumediene, Algiers, Algeria*

[2]*Laboratoire Géosciences- University Montpellier 2- CNRS, Montpellier, France*

1. Introduction

The airborne Gamma Ray (GR) measurements have been used since decades in geophysical research. The airborne measurement of gamma radiation emitted by naturally occurring elements finds applications in: geological mapping (Graham and Bonham-Carter, 1993; Jaques *et al.*, 1997; Doll *et al.*, 2000, Aydin *et al.*, 2006; Sulekha Rao *et al.*, 2009), regolith and soil mapping (Cook *et al.*, 1996; Wilford *et al.*, 1997; Bierwirth and Welsh, 2000), mineral exploration (Brown *et al.*, 2000), and hydrocarbon research (Matolín and Stráník, 2006).

Potassium (K), Uranium (U) and Thorium (Th) are the three most abundant, naturally occurring radioactive elements. The K element is the main component of mineral deposits, while Uranium and Thorium are present in trace amounts, as mobile and immobile elements, respectively. The concentration of these different radioelements varies between different rock types, thus the information provided by a gamma-ray spectrometer can be exploited for needs of the rocks cartography. The obtained maps allow to localize radioelement anomalies corresponding to zones disrupted by a mineralizing system.

The approach presented in this chapter deepens the results derived from the conventional study. It consists on a mono(two)-dimensional fractal analysis of natural radioactivity measurements recorded over the Hoggar area (Algeria).

The natural radioactivity measurements, like other geophysical signals, contain a deterministic and a stochastic components. The former part holds information related to the regional aspect, while the latter reflects the local heterogeneities. As the raw spectrometric data need to be processed before any exploitation, the stochastic component can be altered and some information about heterogeneities is lost.

Here, we show first the fractal behavior of the analyzed GR measurements. In addition, it is demonstrated that this behavior is not affected by all the pre-processing operations (spectrometric corrections and 2D-interpolations). The corrections are not then necessary. Since the analyzed data exhibit a fractal exponent varying with the spatial position, they are modeled as paths of multifractional Brownian motions (mBms) (Peltier and Lévy-Véhel, 1995).

The local Hölder exponent (or local regularity) maps obtained from the GR data recorded in the K, Th and U channels, using a multiple filter technique that we generalize to a 2D-case, exhibit almost an identical image. Besides, they allow to locate the faults affecting the studied zone.

2. Regional geology

The Hoggar is a large shield area covering approximately 550,000 km². It includes an important surface of the Tergui shield, prolonged in South-east, in Mali, by the solid mass of Iforas and in the East, in Niger, by the solid mass of Aïr (Fig. 1).
The Hoggar belongs to the Trans-Saharan pan-African chain (Cahen *et al.*, 1984, Liégeois *et al.*, 1994). It is crossed by two major submeridian faults, located at longitudes 4°50' and 8°30', which delimit three longitudinal compartments (Eastern, Central and Western), with different structural and lithological characteristics. This geological configuration resulted by an extreme E-W compression, during the pan-African (600 My), of the Touareg shield by two rigid plates: the Western African craton and the Eastern African craton (Bertrand and Caby, 1978; Black *et al.*, 1979).

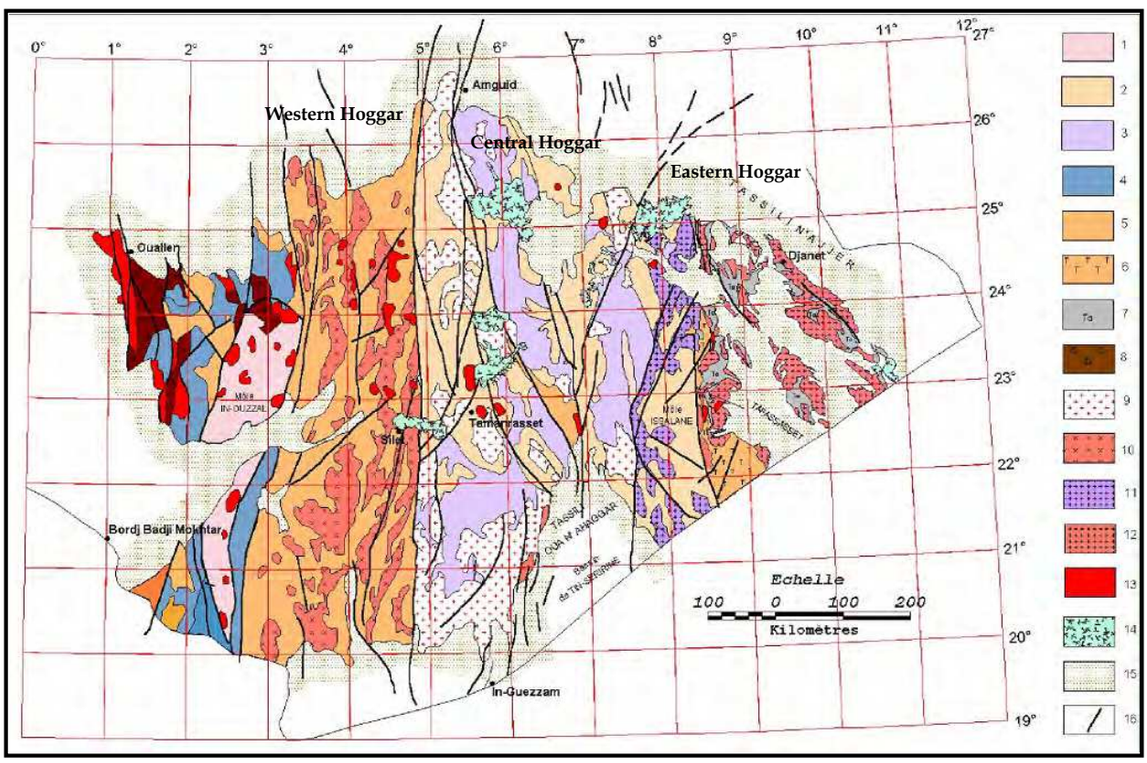

1 - Archaean granulites; **2** - Gneiss and metasediments, series of Arechchoum (Pr1); **3** - Gneiss with facies amphibole, series of Aleskod (Pr2); **4** - Indif. gneiss (Pr3); **5** - Pharusian Greywackes; **6** - Arkoses and conglomerates, series of Tririne (Pr4); **7** - Volcano-sediments of Tafassasset (Pr4); **8** - Molasses (purple series) of Cambrian; **9** – Pan-African syn-orogenic granites; **10** - Pan-African Granites; **11** - Pan-African post-orogenic granites; **12** - Granites of Eastern Hoggar; **13** - Late pan-African Granites; **14** - Basalts and recent volcanism; **15** - Paleozoic cover; **16** - Fault.

Fig. 1. A simplified geological map of the Hoggar (Caby *et al.*, 1981, modified)

3. Overview on the analyzed GR measurements

The analyzed GR measurements are recorded during a magneto-spectrometric survey accomplished, between 1971 and 1974 over the Hoggar, for the purpose of the mining research and the regional geological mapping.
The technical characteristics of the survey are:

- Two types of planes :
  - Douglas DC-3.
  - Aero Commander.
- Navigation System: Doppler type A DRA-12
- Magnetic Compass of type Sperry CL 2, with a resolution of 1°.
- Radar altimeter with an accuracy of 30 feet (type Honeywell Minneapolis).
- Camera with a continuous 35 mm-film
- Acquisition system of data (type Lancer) for the recording of the numerical data on magnetic tapes of 1/2".
- Two types of graphic recorders: with 2 and 6 channels for the graphic monitoring of the magnetic and spectrometric profiles respectively.
- Two types of magnetometers:
  - Magnetometer with optical pumping with the Cesium (model VARIAN) of resolution of 0.02 NT (nano Tesla).
  - Magnetometer Flow-gate of a resolution of 0.5 NT.
- NaI(Tl) spectrometer with four (04) channels: Total Count (TC), Uranium (U), Thorium (Th) and Potassium (K).

The parameters of airborne spectrometric survey carried out over the Hoggar area are:

- The average of the flight height is fixed at 500 feet (approximately 150 m).
- The direction of the profiles: perpendicular to the geological structures.
- The distance between lines varies from 2 to 5 kilometers according to the areas, but on average it is about two kilometers.
- The distance between the observation points is approximately 46.2 m (152 feet).

4. Corrections of the airborne natural activity measurements

The measurements acquired during an airborne spectrometric survey can not be exploited in a raw state, but need to be corrected mainly from aircraft background, stripping (or Compton) effect and height effect (IAEA, 2003).

Background corrections

There are three components of the background correction:

- The instrument background (called ''aircraft background'' in airborne gamma spectrometry),
- The cosmic background arisen from the reaction of primary cosmic radiation with atoms and molecules in the upper atmosphere.
- The effect of atmospheric radon. In portable or car-borne gamma ray surveys, the background component is usually small relative to the signal from the ground.

The observed count rates in the four channels: Total Count (TC), Potassium (K), Uranium (U) and Thorium (Th), are corrected for the background effects using the following formulae:

$$\begin{aligned} TC_{corr} &= TC_{obs} - BC_{TC} \\ K_{corr} &= K_{obs} - BC_K \\ U_{corr} &= U_{obs} - BC_U \\ Th_{corr} &= Th_{obs} - BC_{Th} \end{aligned} \quad (1)$$

where all these values are expressed in counts per second (cps).
TC_{corr}, K_{corr}, U_{corr} and Th_{corr} : Values of the corrected count rates in the four channels,
TC_{obs}, K_{obs}, U_{obs} and Th_{obs} : Values of the observed count rates in the four channels,
BC_{TC}, BC_K, BC_U and BC_{Th} : Values of the background correction in the four channels. In this case, the estimated values are (Groune, 2009): BC_{TC} = 250 cps, BC_K = 72 cps, BC_U = 17 cps and BC_{Th} = 5 cps.

Stripping correction

This correction, also known as the channel interaction correction, consists of removing ('strips') count rates from each of the K, U and Th for gamma rays not originating from the radioelement or decay series being monitored. For example, Th series gamma rays appear in both the U and K channels, and U series gamma rays appear in the K channel. The corrections are given by:

$$\begin{aligned} U_{corr} &= U_{obs} - \alpha\, Th_{obs} \\ K_{corr} &= K_{obs} - \beta\, Th_{obs} - \gamma\, U_{obs} \end{aligned} \quad (2)$$

K_{corr} and U_{corr} : Values of the corrected count rates in the K and U channels respectively.
K_{obs}, U_{obs} and Th_{obs} : Values of the observed count rates in the K, U and Th channels respectively.
α, β and γ : Stripping coefficients. The used coefficients in this application are (Aeroservice, 1975): $\alpha = 0.45$, $\beta = 0.59$ and $\gamma = 0.94$.

Height correction

This correction is applied only on airborne gamma spectrometric measurements. The gamma radiation decreases exponentially with the elevation. Since the height of the aircraft changes continuously, the airborne Gamma Ray spectrometric data need to be corrected to a nominal survey height above the ground.

$$\begin{aligned} TC_{corr} &= TC_{obs} \exp\left[\mu_{TC}\left(h - h_0\right)\right] \\ K_{corr} &= K_{obs} \exp\left[\mu_K\left(h - h_0\right)\right] \\ U_{corr} &= U_{obs} \exp\left[\mu_U\left(h - h_0\right)\right] \\ Th_{corr} &= Th_{obs} \exp\left[\mu_{Th}\left(h - h_0\right)\right] \end{aligned} \quad (3)$$

TC_{corr}, K_{corr}, U_{corr} and Th_{corr} : Values of the corrected count rates in the four channels,
TC_{obs}, K_{obs}, U_{obs} and Th_{obs} : Values of the observed count rates in the four channels,
h : Real survey height ,
h_0 : Nominal survey height (h_0=150 m),
μ_{TC}, μ_K, μ_U and μ_{Th} : Linear attenuation coefficients in the four channels. The estimated values of these coefficients are (Groune, 2009) : μ_K = 6.8617 10^{-3} m^{-1}, μ_U = 6.3726 10^{-3} m^{-1} , and μ_{Th} = 5.2247 10^{-3} m^{-1} . The μ_{TC} is calculated as the approximate average of the three coefficients: μ_{TC} = 6.56 10^{-3} m^{-1} .

5. Impact of the pre-processings on the fractal properties of the airborne gamma ray measurements

Once all the corrections are applied, the corrected measurements grid is regrided using two-dimensional interpolation algorithms to get a regular sampled grid which is processed by a local regularity analysis.

The set of operations (corrections and interpolations) affects the stochastic component of the raw airborne spectrometric measurements, which holds information about heterogeneities. Therefore the fractal properties of the raw data may be changed.

In the first stage, we have obtained the ''corrected'' and the ''corrected and interpolated'' data grids from the ''raw'' grid data corresponding to the measurements of the three channels: K, Th and U. The 2D-interpolation algorithms used in this study are: the triangle-based linear, the triangle-based cubic and the nearest neighbor interpolation algorithms. Since the results obtained by the different interpolation methods are close, only those related to the triangle-based linear algorithm are presented.

First, five vertical profiles are extracted from the three considered grids (''raw'', ''corrected'' and ''corrected and interpolated '' grids) from the measurements of the three channels (Fig.2). The Fourier amplitude spectrum and the local Hölder exponent $H(x)$ are computed for each data profile.

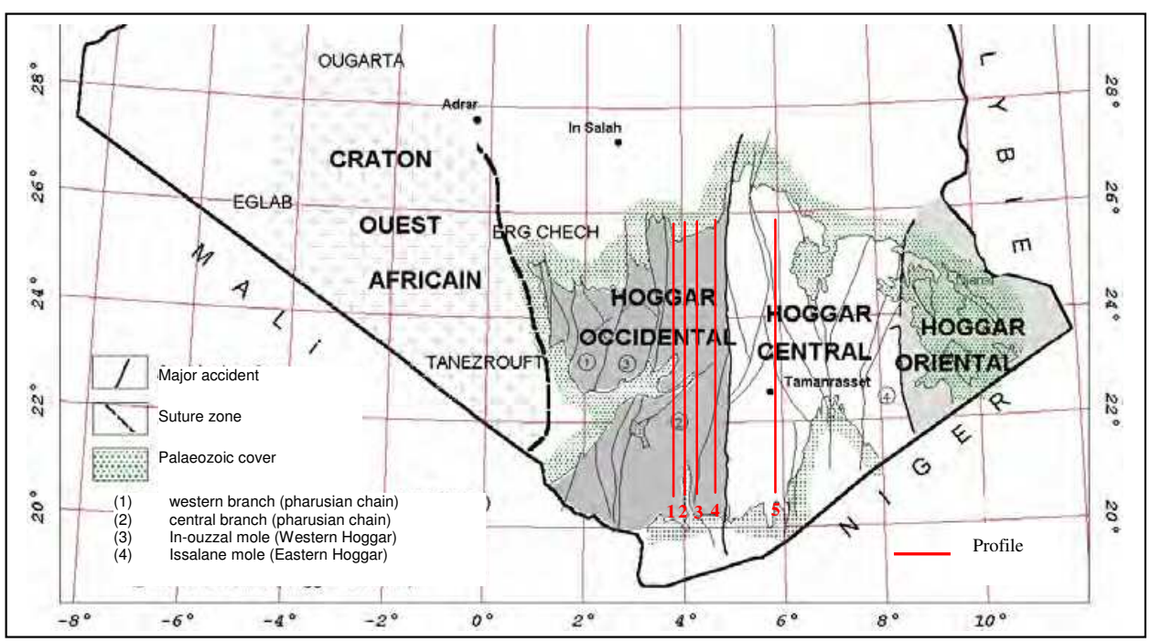

Fig. 2. Position of the five profiles extracted from the GR measurements (in red).
(The geological map of the Hoggar, from Caby *et al.*, 1981).

Regarding the computation of $H(x)$, we need a sequence $S_{k,n}(i)$ defined by the local growth of the increment process:

$$S_{k,n}(i) = \frac{m}{n-1} \sum_{j \in [i-k/2, i+k/2]} \left| X(j+1) - X(j) \right|, \; 1<k<n \tag{4}$$

where n is the signal X length, k is a fixed window size, and m is the largest integer not exceeding n/k.
The local Hölder function $H(x)$ at point

$$x = \frac{i}{n-1} \tag{5}$$

is given by (Peltier and Lévy-Véhél, 1994, 1995; Muniandy *et al.*, 2001 ; Li *et al.*, 2007, 2008; Gaci *et al.*, 2010):

$$\hat{H}(i) = -\frac{\log\left[\sqrt{\pi/2}\; S_{k,n}(i)\right]}{\log\ (n-1)} \tag{6}$$

From figure 3, it can be seen that all the calculated amplitude spectra, represented in a log-log plan, decay algebraically, the analyzed data exhibit then a fractal behavior. Moreover, the latter is described by a Hölder exponent varying with the latitude of the measure. Hence the data can be considered as paths of multifractional Brownian motions (mBms) (Peltier and Lévy-Véhel, 1995; Gaci *et al.*, 2011).
A significant result deserves to be noted is the fact that the spectra obtained from the ''raw'', ''corrected'' and ''corrected and interpolated'' measurements display a similar form. That is the applied operations (corrections and interpolations) do not affect the fractal aspect of the raw data.

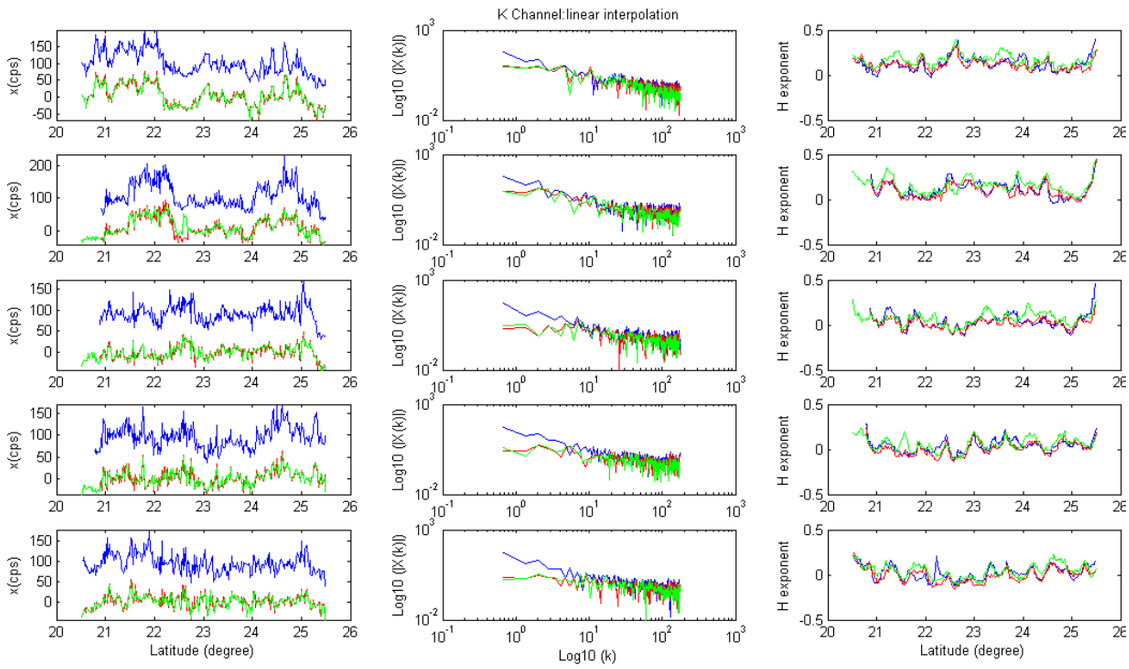

a)

Fig. 3. (Continued)

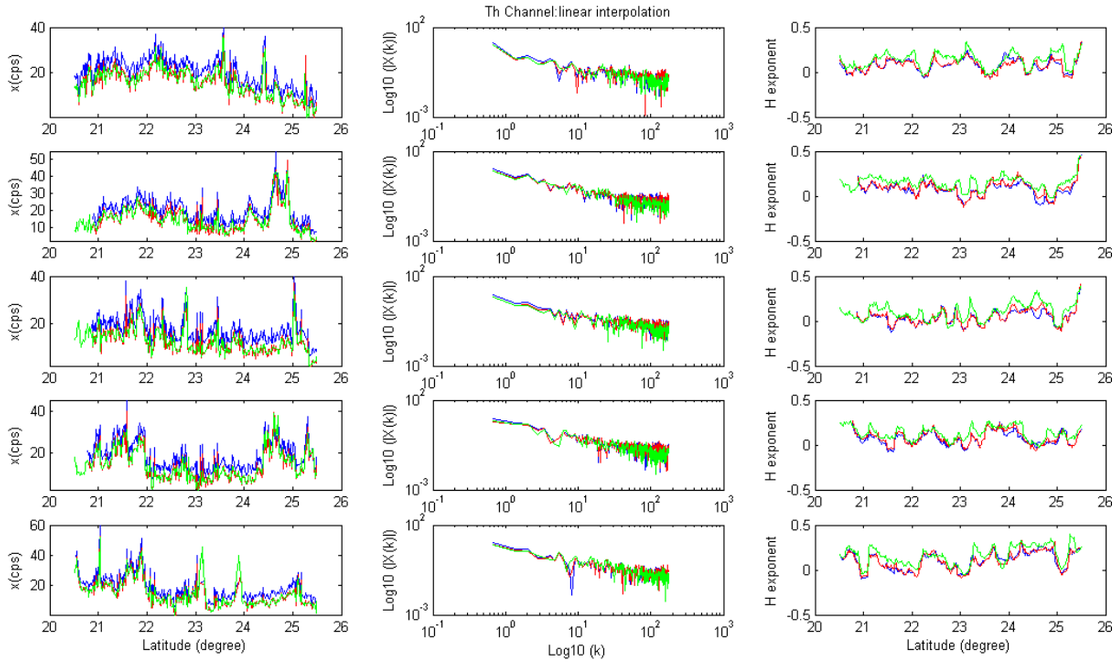

b)

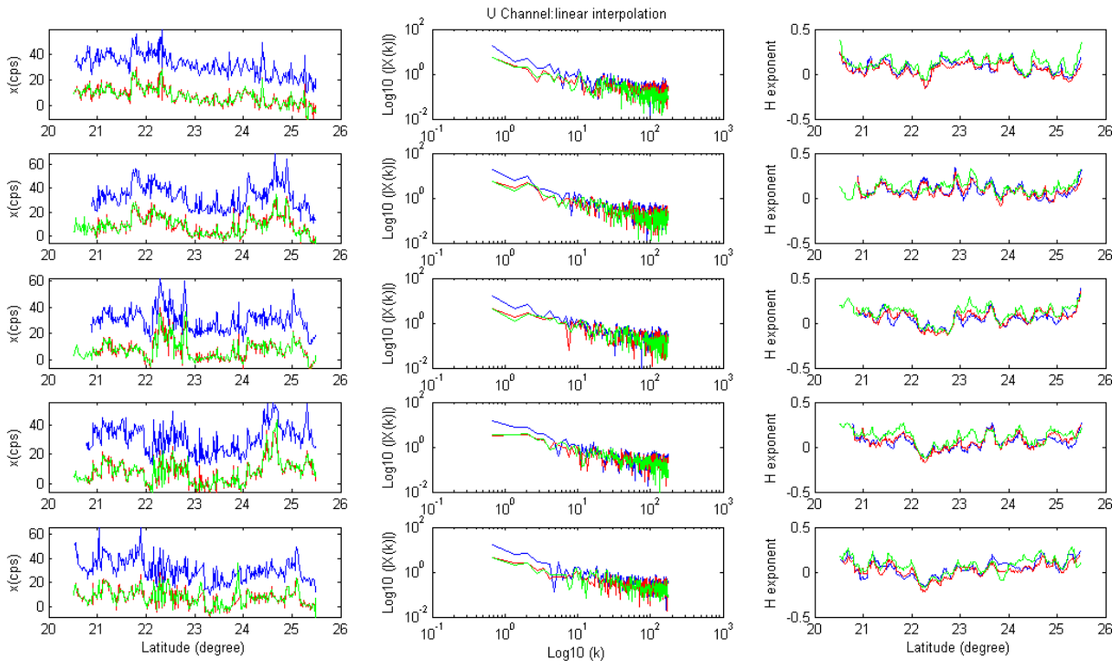

c)

On the left, the measurements profile, in the middle the module of the amplitude spectrum of the measurements profile versus the wavenumber (rad/degree) in the log-log scale, and on the right, the local Hölder function.
The raw data (blue), the corrected data (red) and the corrected and interpolated data (green).

Fig. 3. Investigation of the impact of pre-processings on the fractal properties of the five profiles of the airborne GR data recorded in the channel: (a) K, (b) Th, (c) U.

Moreover, the estimated Hölder functions obtained from the three types of measurements present very close values. Again, we confirm that the fractal properties of the raw data are not modified by both pre-processing operations. The implementation of the different 2D-interpolation algorithms illustrates that the choice of the interpolation algorithm has a very slight effect on the estimated *H* value. An important result to be noted: the spectrometric corrections are not necessary for a fractal analysis which can be carried out directly on the raw measurements. By doing so, the stochastic component of the measurements is kept intact.

6. Local regularity analysis of airborne spectrometric data

In this section, we establish local two-dimensional regularity maps, from the interpolated raw GR data measured in the three channels: K, Th and U, using a wavelet-based algorithm via the two-dimensional Multiple Filter Technique (2D MFT). We obtained the latter technique by generalizing the mono-dimensional version (Dziewonski *et al.*, 1969; Li, 1997) to the 2D-case (Gaci, 2011).

6.1 Spectrometric data interpolation

Considering the limitations of the computer's processing capacity, we consider the GR measurements recorded, in the K, Th and U channels, over the zone whose geographical coordinates are defined by: longitude: 3° 13′ 58′′- 6°59′ 26′′ E, and latitude: 20° 27′ 35′′-25° 06′ 37′′ N.

The 2D-interpolation of the raw spectrometric data is performed owing to the kriging algorithm. The interpolated GR grids data related to the K, Th and U channels are illustrated respectively by figures 4, 5 and 6.

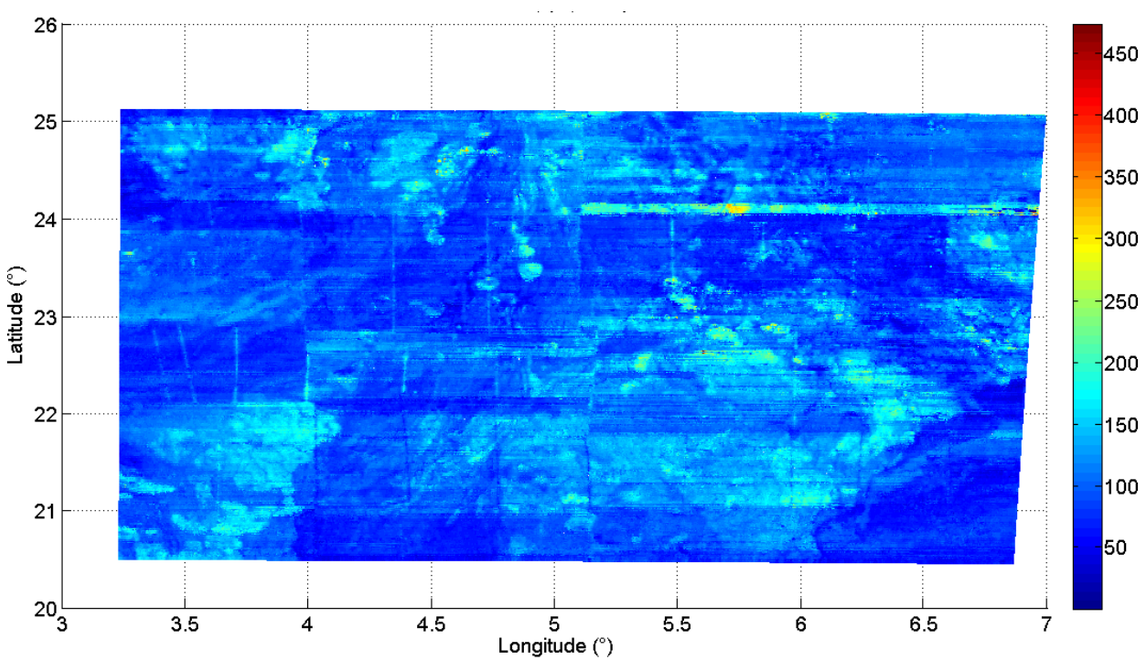

Fig. 4. Interpolated Gamma Ray measurements (in cps) related to the K channel .

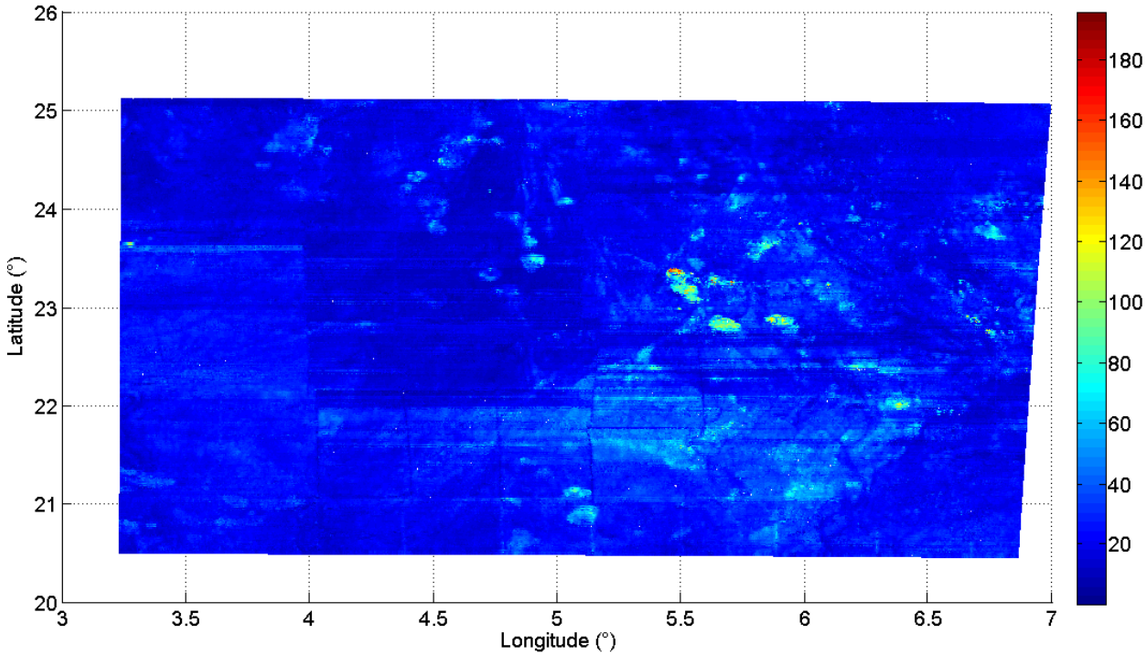

Fig. 5. Interpolated Gamma Ray measurements (in cps) related to the Th channel.

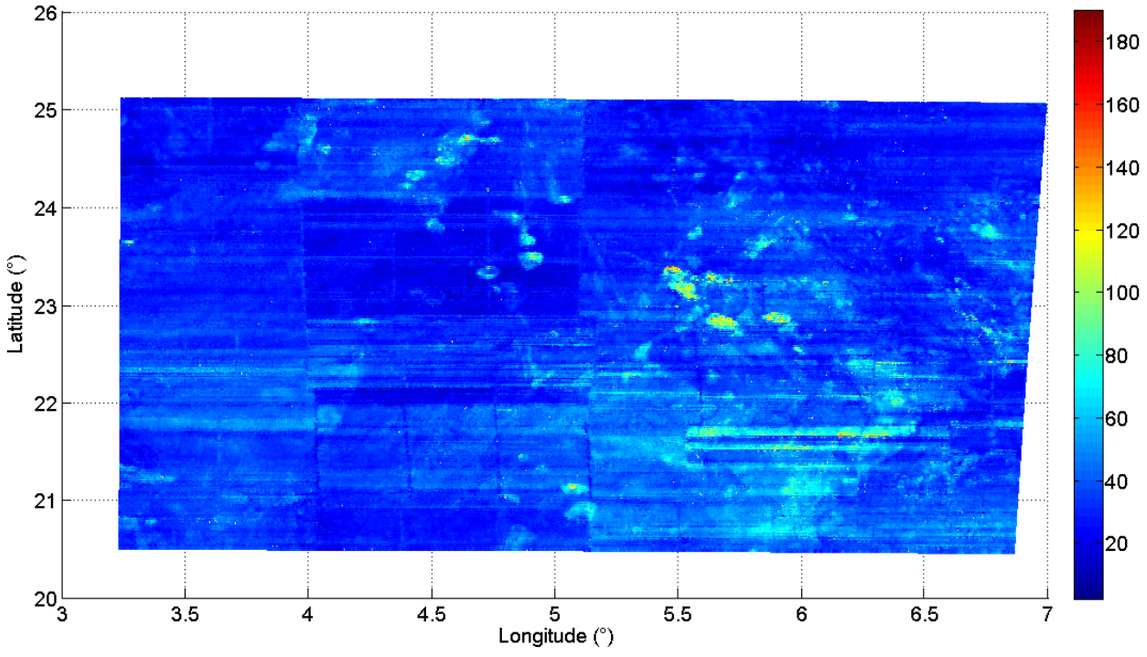

Fig. 6. Interpolated Gamma Ray measurements (in cps) related to the U channel.

6.2 Establishment of local regularity maps from interpolated spectrometric data

Using a wavelet-based algorithm, we estimate Hölder exponent maps, from the interpolated GR measurements recorded in the three channels (K, Th and U).

Recall that the two-dimensional continuous wavelet transform (2D- CWT) is given by a convolution product of a signal $s(x,y)$ and an analyzing wavelet $g(x,y)$ (Chui, 1992; Holschneider, 1995):

$$S(a,b_x,b_y)=\frac{1}{\sqrt{a}}\int_{-\infty}^{\infty}s(x,y)\,\bar{g}\left(\frac{x-b_x}{a},\frac{y-b_y}{a}\right)dx\,dy$$

where "a" is the scale parameter, "b_x " and "b_y" are the respective translations according to X-axis and Y-axis (the symbol " $-$" denotes the complex conjugate).
Alternatively, it can be computed via the Fast Fourier Transform:

$$S(a,b_x,b_y)=FFT^{-1}\left(\hat{s}(\xi,\nu).\sqrt{a}\;\bar{\hat{g}}(a\xi,a\nu)\right)$$

Here, we compute the wavelet coefficients via FFT using the two-dimensional multiple filter technique (2D MFT). The latter technique is obtained by generalizing the one-dimensional version (1D MFT), suggested by Dziewonski et *al.* (1969) and improved by Li (1997), to the two-dimensional case. It consists of filtering a two-dimensional signal using a Gaussian filter $G(k,\xi_n,\nu_m)$ given by (Gaci, 2011):

$$\begin{aligned}G(k,\xi_n,\nu_m)&=G_1(k,\xi_n)G_2(k,\nu_m)\\&=e^{-\alpha\left(\frac{k-\xi_n}{\xi_n}\right)^2}e^{-\alpha\left(\frac{k-\nu_n}{\nu_n}\right)^2}\end{aligned}\tag{7}$$

Where ξ_n and ν_m are variable center angular frequencies (or wavenumbers) of the respective filters $G_1(k,\xi_n)$ and $G_2(k,\nu_m)$. The bandwidths Δk_1 and Δk_2 of both filters are calculated as:

$$\begin{aligned}\Delta k_1&=\xi_2-\xi_1=\beta.Ln(\xi_n)\\\Delta k_2&=\nu_2-\nu_1=\beta.Ln(\nu_m)\end{aligned}\tag{8}$$

Where β is a constant, (ξ_1 , ξ_2) and (ν_1 , ν_2) are respectively the – 3 dB points of the Gaussian filters G_1 and G_2 , respectively.
A fractal surface $s(x,y)$ verifies the self-affinity property (Mandelbrot, 1977, 1982; Feder, 1988) :

$$s(\lambda x,\lambda y)\cong\lambda^H.s(x,y)\,,\ \forall\lambda>0\tag{9}$$

Where H is the Hurst exponent (or the self-affinity parameter). The symbol $\cong$ means the equality of all its finite-dimensional probability distributions.
For sufficiently large values of k, the scalogram, defined as the square of the amplitude spectrum: $P(k,x,y)=|S(k,x,y)|^2$, can be expressed as:

$$P(k,x,y)=P'(x,y).k^{-\beta(x,y)}\propto k^{-\beta(x,y)}\tag{10}$$

Where

$$\beta(x,y)=2H(x,y)+1\tag{11}$$

is the local spectral exponent which is related to the local Hurst (or Hölder) exponent, $H(x,y)$. The spectral exponent $\beta(x,y)$ in each point (x,y) is computed as the slope of the scalogram versus the wavenumber in the log-log plan, the $H(x,y)$ value is then derived using the equation (11).

The implementation of the wavelet-based algorithm, using the generalized multiple filter technique, allows to establish regularity maps from the interpolated GR measurements recorded in the three channels (K, Th and U) (Fig. 7). In order to interpret the resulting maps in terms of geology, a geological map of the studied zone is considered.

The results show that the H maps, derived from the measurements of all the channels, exhibit almost an identical image of the local regularity. By reporting the faults affecting the studied zone on the obtained regularity maps, we remark that the faults locations correspond to local minima of H values. The main accident (the 4°50' fault) is noticeable on almost all the regularity maps. However, the regularity maps present local minima of H values in some places, probably due to less important faults which have to be checked on updated detailed geological maps.

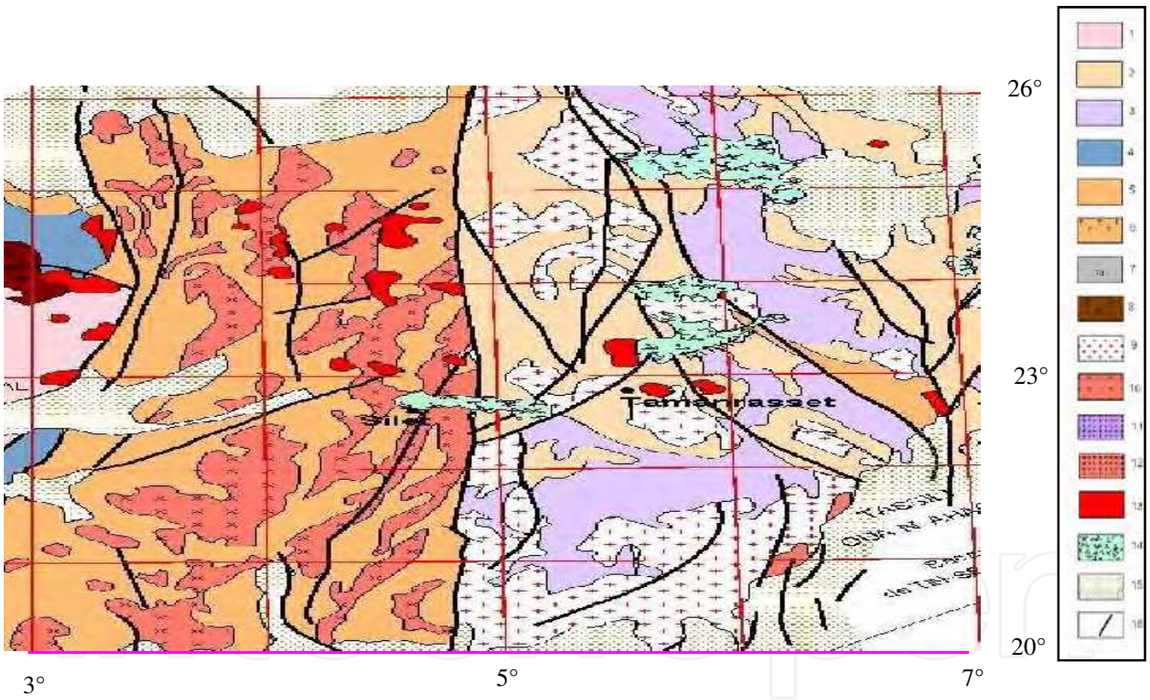

(a) A geological map of the studied zone

1 - Archaean granulites; **2** - Gneiss and metasediments, series of Arechchoum (Pr1); **3** - Gneiss with facies amphibole, series of Aleskod (Pr2); **4** - Indif. gneiss (Pr3); **5** - Pharusian Greywackes; **6** - Arkoses and conglomerates, series of Tririne (Pr4); **7** - Volcano-sediments of Tafassasset (Pr4); **8** - Molasses (purple series) of Cambrian; **9** – Pan-African syn-orogenic granites; **10** - Pan-African Granites; **11** - Pan-African post-orogenic granites; **12** - Granites of Eastern Hoggar; **13** - Late pan-African Granites; **14** - Basalts and recent volcanism; **15** - Paleozoic cover; **16** - Fault.

Fig. 7. (Continued)

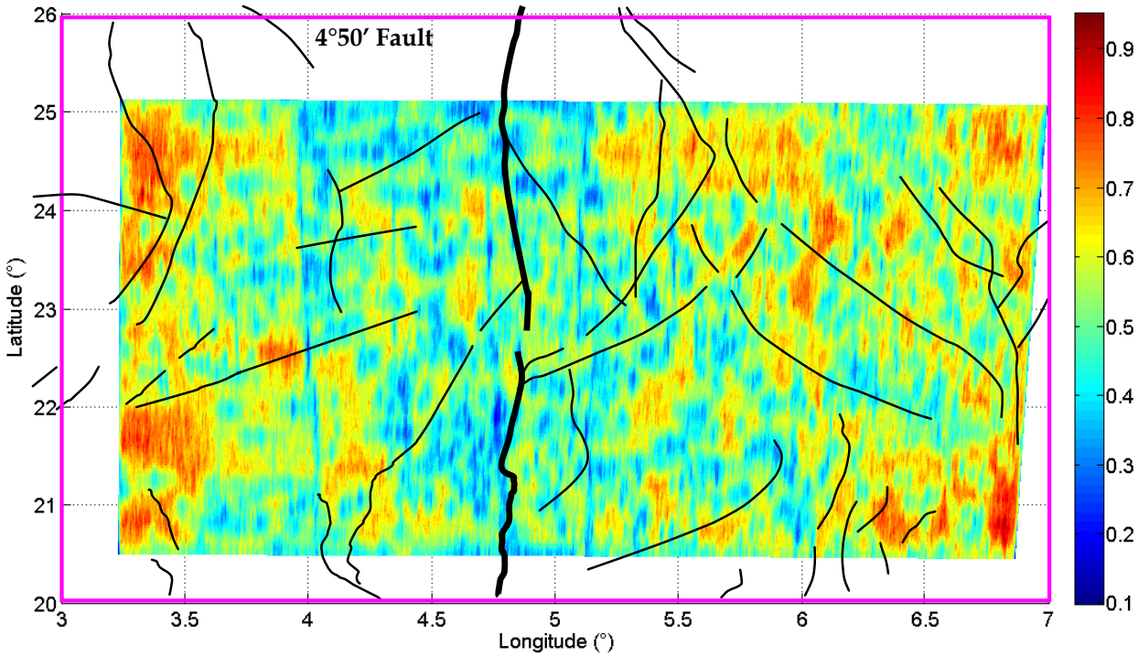

(b) Regularity map obtained from GR measured in the K channel

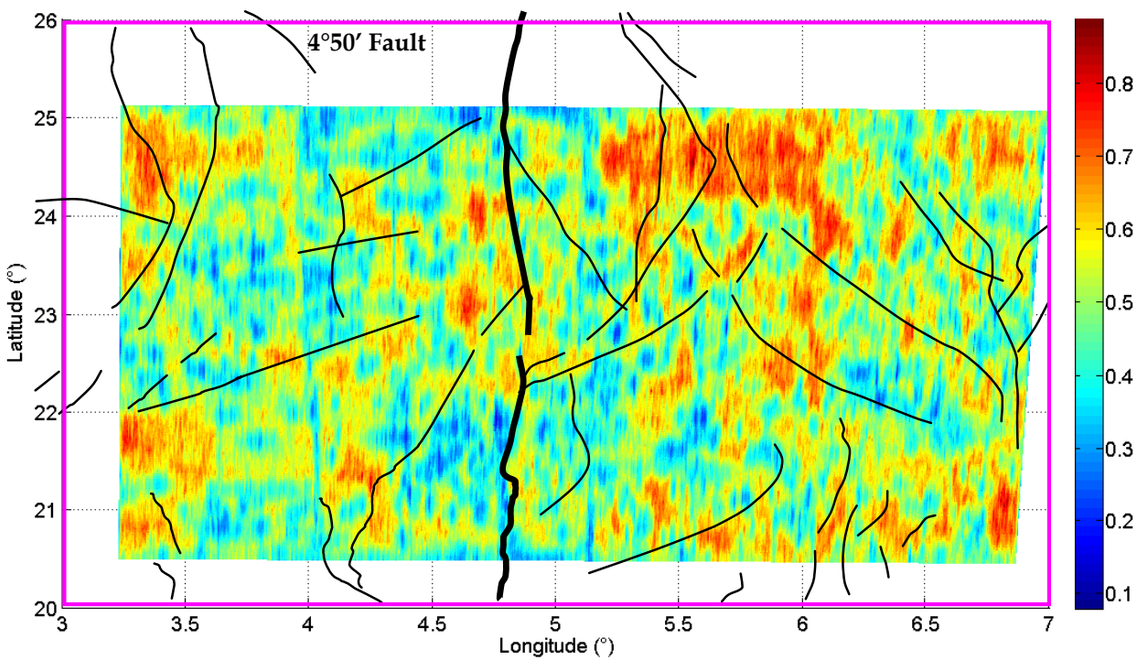

(c) Regularity map obtained from GR measured in the Th channel

Fig. 7. (Continued)

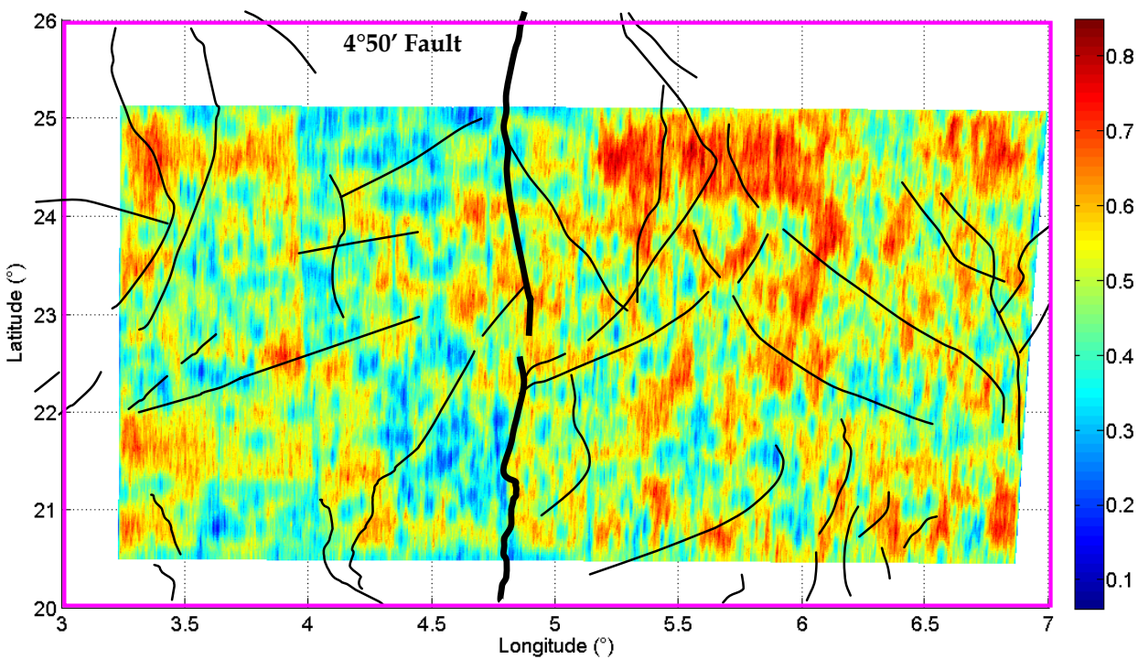

(d) Regularity map obtained from GR measured in the U channel

Fig. 7. Comparison of regularity maps obtained from GR measured in (b)K, (c)Th and (d)U channel and the geological map of the studied zone (a).
The faults affecting the studied area are projected on the *H* maps.

Now, we try to establish a correspondence between the obtained regularity maps and the geological map of the area. Since the obtained regularity maps are similar, we choose that estimated from the measurements recorded in the Th channel. Then, on the considered geological map and *H* map, we delimit in dotted lines the geological formations; the same color corresponds to the same geological facies (Fig. 8). These two maps show that a considered lithology is not characterized by the same value of the *H* coefficient. These obtained preliminary results reveal that the *H* value can not be used as an attribute to characterize lithology, while it could be used for the recognition and the establishment of the network faults.

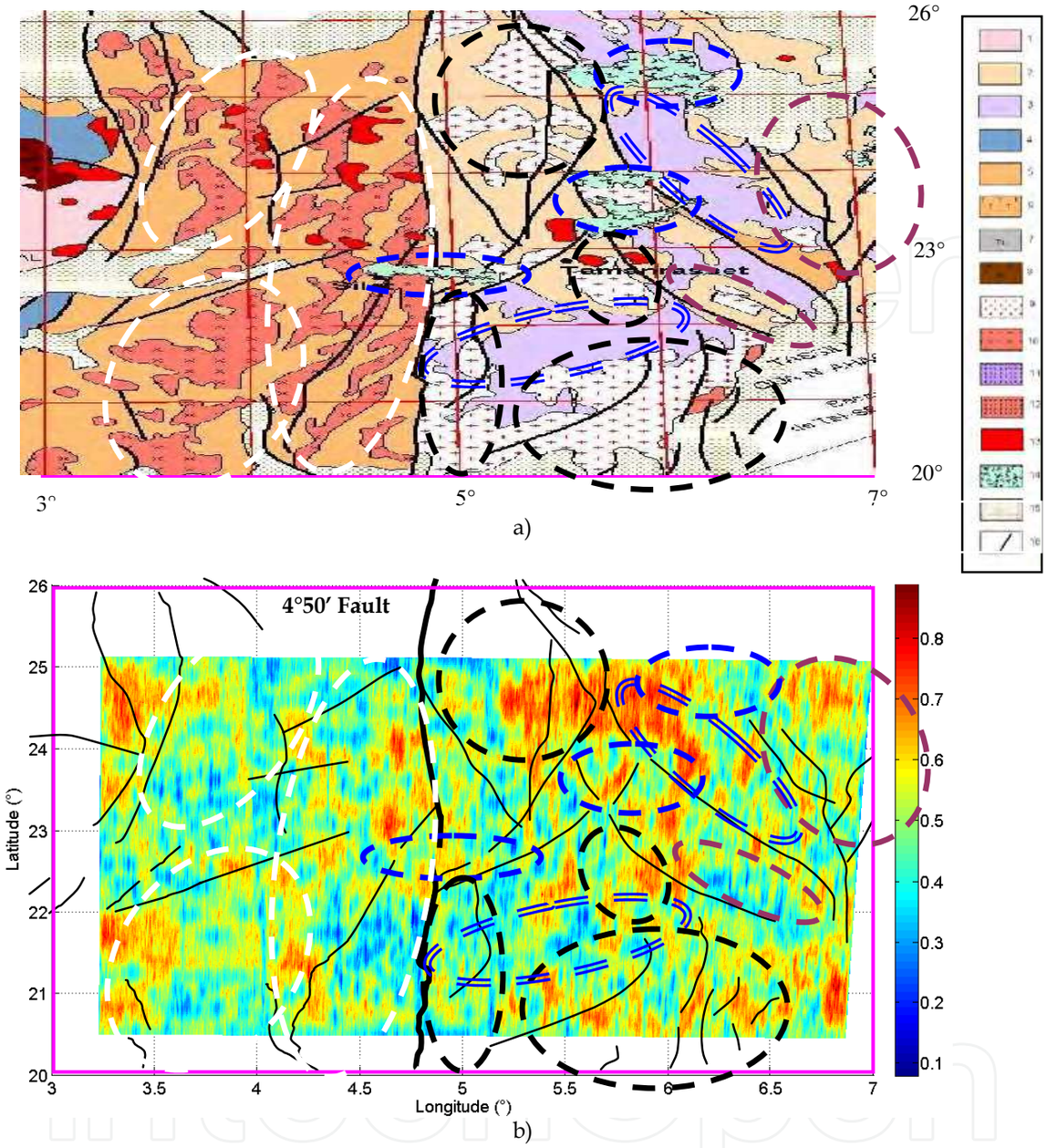

1 - Archaean granulites; **2** - Gneiss and metasediments, series of Arechchoum (Pr1); **3** - Gneiss with facies amphibole, series of Aleskod (Pr2); **4** - Indif. gneiss (Pr3); **5** - Pharusian Greywackes; **6** - Arkoses and conglomerates, series of Tiririne (Pr4); **7** - Volcano-sediments of Tafassasset (Pr4); **8** - Molasses (purple series) of Cambrian; **9** – Pan-African syn-orogenic granites; **10** - Pan-African Granites; **11** - Pan-African post-orogenic granites; **12** - Granites of Eastern Hoggar; **13** - Late pan-African Granites; **14** - Basalts and recent volcanism; **15** - Paleozoic cover; **16** - Fault.

Fig. 8. Correlation of the regularity map (b) obtained from the GR measurements recorded in the Th channel with the geological map of the studied zone (a). The ellipses in dotted lines delimit the geological formations: black (pan-African syn-orogenic granites), white (pan-African granites), simple blue line (basalts and recent volcanism), doubled blue line (gneiss with amphibole facies), brown (gneiss and metasediments).

7. Conclusion

This study presents a regularity analysis undertaken on the airborne spectrometric natural radioactivity measured, in three channels: K, Th and U, over the Hoggar area (Algeria). It reveals that the investigated data exhibit fractal properties depending on the spatial measurement location, thus can be modeled using multifractional Brownian motions. As the spectrometric corrections do not affect these properties, the regularity analysis can be carried out directly on the interpolated raw measurements.
The Hölder exponent maps, obtained from the Gamma Ray measurements recorded in the three channels, show a similar local regularity. Besides, a strong correlation is derived between the *H* exponent values and the faults locations. Indeed, a fault corresponds to local minima *H* values, the *H* exponent value can then be used to identify the faults. However, it does not allow to characterize the lithological facies.

8. Acknowledgements

This work was supported by the Algerian –French program CMEP—PHC Tassili N°09 MDU 787.

9. References

Aeroservice Corporation (1975) Aero-magneto-spectrometric survey of Algeria. Final report, 3 volumes, Houston, Philadelphia.

Aydin, I.; Selman Aydoğan, M. ; Oksum, E. & Koçak, A. (2006) An attempt to use aerial gamma-ray spectrometry results in petrochemical assessments of the volcanic and plutonic associations of Central Anatolia (Turkey). Geophys. J. Int. Vol. 167, pp. 1044–1052.

Bertrand, J.M.L. & Caby, R. (1978) Geodynamic evolution of the pan-african orogenic belt: A new interpretation of the Hoggar shield (Algerian Sahara), Geol. Rundschman, Vol. 67, pp. 357-388.

Bierwirth, P.N., & Welsh, W.D. (2000) Delineation of Recharge Beds in the Great Artesian Basin Using Airborne Gamma Radiometrics and Satellite Remote Sensing, Bureau of Rural Sciences, Kingston, Australia.

Black, R.; Caby, R. & Moussine-Pouchkine, A. (1979) Evidence for late Precambrian plate tectonics in west Africa, Nature, Vol. 278, pp. 223-227.

Brown, W.M. ; Gedeon, T.D. ; Groves, D.I. & Barnes, R.G. (2000) Artificial neural networks: a new method for mineral prospectivity mapping. Australian Journal of Earth Sciences, Vol. 47, 757–770.

Caby, R.; Bertrand, J.M.L. & Black, R. (1981) Pan-African closure and continental collision in the Hoggar-Iforas segment, central Sahara. in Kroner A (ed) Precambrian Plate Tectonics, Elsevier, Amst. pp. 407-434.

Cahen, L., Snelling, N.J. ; Delhal, J. & Vail J.R. (1984) The geochronology and evolution of Africa, Clarendon Press, Oxford., 512 pp.

Chui, C.K. (1992) An introduction to wavelets. Academic Press.

Cook, S.E.; Corner, R.J.; Groves, P.R. & Grealish, G.J. (1996) Use of airborne gamma radiometric data for soil mapping, Australian Journal of Soil Research. Vol. 34, No.1, pp. 183–194.

Doll, W.E.; Nyquist, J.E.; Beard, L.P. & Gamey,T.J. (2000) Airborne geophysical surveying for hazardous waste site characterization on the Oak Ridge Reservation, Tennessee, Geophysics. Vol. 65, pp. 1372–1387.

Dziewonski, A.; Bloch, S. & Landisman, M. (1969) A technique for the analysis of transient seismic signals: *Bull. Seismol. Soc. Am.*, Vol. 59, pp. 427–444.

Feder, J. (1988). Fractals, p. 283, Plenum (Ed.), New York.

Gaci, S.; Zaourar, N. ; Hamoudi, M. & Holschneider, M. (2010). Local regularity analysis of strata heterogeneities from sonic logs. *Nonlin. Processes Geophys.*, Vol. 17, pp. 455-466, http: www.nonlin-processes-geophys.net/17/455/2010/doi:10.5194/npg-17-455-2010

Gaci, S. (2011). Multifractional analysis of geophysical signals (*in French*). PhD thesis. Univ. of Sciences and Technology Houari Boumdiene (Algeria).

Gaci, S.; Zaourar, N.; Briqueu, L. & Djeddi, M., (2011). Fractal characterization of natural radioactivity measurements in the Hoggar region (Algeria), EGU Proceedings, Vienna, Austria.

Graham, D.F. & Bonham-Carter, G.F. (1993) Airborne radiometric data: A tool for reconnaissance geological mapping using a GIS, Photogrammetric Engineering and Remote Sensing, Vol. 59, pp. 1243–1249.

Groune D. (2009) Magneto-spectrometric analysis of the airborne geophysical data of the large Pharusian ditch (Western Hoggar). Msc thesis, University of Boumerdes. Algeria (in French).

Holschneider, M. (1995). Wavelets: an Analysis Tool. Clarendon. Oxford, England.

International Atomic Energy Agency (IAEA) (2003) Guidelines for radioelement mapping using gamma ray spectrometry data. Vienna, Austria. 179 pp.

Jaques, A.L.; Wellman, P.; Whitaker, A. & Wyborn, D. (1997) High-resolution geophysics in modern geological mapping, AGSO Journal of Australian Geology and Geophysics. Vol. 17, No. 2, pp. 159–173.

Li, X-P (1997). Decomposition of vibroseis data by the multiple filter technique. *Geophysics*, Vol. 62, No. 3, pp. 980–991.

Li, M.; Lim, S.C. ; Hu, B-J. & Feng, H. (2007). Towards describing multi-fractality of traffic using local Hurst function. *Lecture Notes in Computer Science*, Vol. 4488, pp. 1012-1020.

Li, M.; Lim, S.C. & Zhao, W. (2008). Investigating multi-fractality of network traffic using local Hurst function, Advanced Studies in Theoretical Physics, Vol. 2, No. 10, pp. 479–490.

Liégeois, J. P.; Black, R.; Navez, J. & Latouche, L. (1994) Early and late Pan-African orogenies in the Aïr assembly of terranes (Tuareg shield, Niger), Precambrian Research, Vol. 67, No. 1-2, pp.59-88.

Mandelbrot, B.B. (1977). Fractals : Form, Chance and Dimensions. Freeman, San Francisco.

Mandelbrot, B.B. (1982) The Fractal Geometry of Nature. Freeman, San Francisco.

Matolín, M. & Stráník, Z. (2006) Radioactivity of sedimentary rocks over the Ždánice hydrocarbon field. Geophys. J. Int., Vol. 167, pp. 1491–1500.

Muniandy, S.V.; Lim, S.C. & Murugan, R. (2001). Inhomogeneous scaling behaviors in Malaysian foreign currency exchange rates, Physica A, Vol. 301, No. 1–4, pp. 407–428, 2001.

Peltier, R.F. & Lévy-Véhel, J. (1994). A New Method for Estimating the Parameter of Fractional Brownian motion, Technical report, INRIA RR 2396.

Peltier, R.F. & Lévy-Véhel, J. (1995). Multifractional Brownian Motion: Definition and preliminary results, Technical report, INRIA RR 2645.

Sulekha Rao, N. ; Sengupta, D. ; Guin, R. & Saha S. K. (2009) Natural radioactivity measurements in beach sand along southern coast of Orissa, eastern India. Environ Earth Sci. Vol. 59, pp. 593–601.

Wilford, J.R.; Bierwirth, P.N. & Craig, M.A. (1997) Application of airborne gamma-ray spectrometry in soil/regolith mapping and applied geomorphology, Journal of Australian Geology and Geophysics, Vol. 17, No. 2, pp. 201–216.

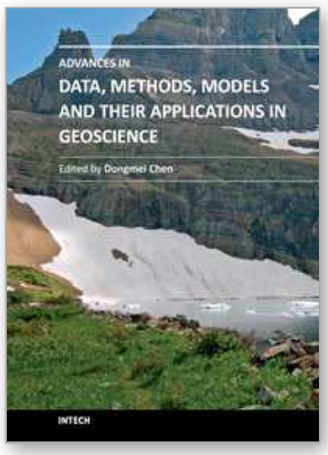

Advances in Data, Methods, Models and Their Applications in Geoscience

Edited by Dr. DongMei Chen

ISBN 978-953-307-737-6
Hard cover, 336 pages
Publisher InTech
Published online 22, December, 2011
Published in print edition December, 2011

With growing attention on global environmental and climate change, geoscience has experienced rapid change and development in the last three decades. Many new data, methods and modeling techniques have been developed and applied in various aspects of geoscience. The chapters collected in this book present an excellent profile of the current state of various data, analysis methods and modeling techniques, and demonstrate their applications from hydrology, geology and paleogeomorphology, to geophysics, environmental and climate change. The wide range methods and techniques covered in the book include information systems and technology, global position system (GPS), digital sediment core image analysis, fuzzy set theory for hydrology, spatial interpolation, spectral analysis of geophysical data, GIS-based hydrological models, high resolution geological models, 3D sedimentology, change detection from remote sensing, etc. Besides two comprehensive review articles, most chapters focus on in-depth studies of a particular method or technique.

InTech Europe
University Campus STeP Ri
Slavka Krautzeka 83/A
51000 Rijeka, Croatia
Phone: +385 (51) 770 447
Fax: +385 (51) 686 166
www.intechopen.com

InTech China
Unit 405, Office Block, Hotel Equatorial Shanghai
No.65, Yan An Road (West), Shanghai, 200040, China
中国上海市延安西路65号上海国际贵都大饭店办公楼405单元
Phone: +86-21-62489820
Fax: +86-21-62489821

IntechOpen